Bryan Gosselin, Raphael Dutour, Julie Janssens, Ivan Jabin, and Gilles Bruylants.

"Repurposing Lateral Flow Assays as a Versatile and Rapid Characterization Tool for Bioconjugation of Nanoparticles."

Bioconjugate Chemistry, 2024. DOI: 10.1021/acs.bioconjchem.4c00589.

Repurposing Lateral Flow Assays as a Versatile and Rapid Characterization Tool for Bioconjugation of Nanoparticles

Bryan Gosselin,[†,‡] *Raphael Dutour,*[†] *Julie Janssens,* [†,‡] *Ivan Jabin,*[‡,*] *and Gilles Bruylants*[†,*]

[†] Engineering of Molecular NanoSystems, Ecole Polytechnique de Bruxelles, Université libre de Bruxelles (ULB), avenue F. D. Roosevelt 50, CP165/64, B-1050 Brussels, Belgium

[‡] Laboratoire de Chimie Organique, Université libre de Bruxelles (ULB), Avenue F. D. Roosevelt 50, CP160/06, B-1050 Brussels, Belgium

Ivan.Jabin@ulb.be; Gilles.Bruylants@ulb.be

TOC

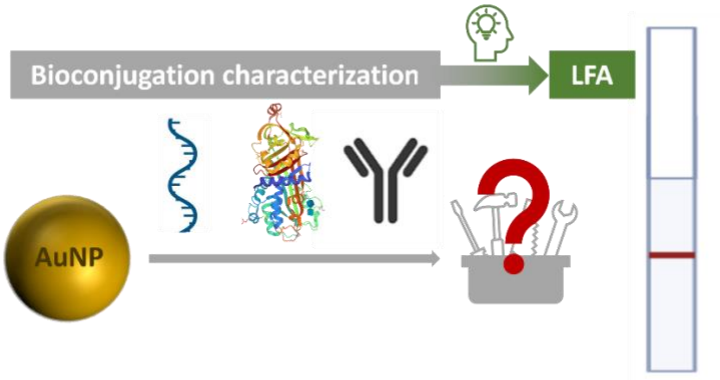

KEYWORDS: Lateral flow assays – Bioconjugation – Nanoparticles – Quality control analysis – Covalent coupling

1. Abstract

This study explores the use of lateral flow assays (LFAs), recognized for their simplicity and ease-of-use, as a tool for characterizing nanoparticles functionalized with various biomolecules (e.g., proteins, antibodies and nucleic acids). A half-strip model system was developed using ovalbumin (OVA) conjugated to gold nanoparticles (AuNPs). The characterization results obtained with LFAs were compared to those from traditional methods such as infrared spectroscopy and fluorescence labelling. The advantages of LFAs in characterizing such conjugated nanosystems were clearly demonstrated. The use of half-strip assays could not only confirm the presence of OVA on AuNPs but also enable the quantification of OVA bound per

nanoparticle, offering a rapid and quantitative characterization method. Additionally, the assay showcased its versatility, as it was successfully applied to optimize the covalent coupling conditions of OVA on AuNPs, as well as to differentiate between covalently bound and adsorbed proteins. Furthermore, LFAs were employed to detect antibodies on functionalized nanoparticles, optimize their coupling to a newly developed organic coating, and confirm both the grafting of nucleic acids onto the surface and their pairing with complementary strands. These findings underscore the remarkable adaptability of LFAs for characterizing diverse nanoconjugates. Overall, LFAs stand out as a versatile and accessible tool for characterizing complex bioconjugated nanosystems, making them highly suitable for rapid Quality Control (QC) analysis and bioconjugation optimization.

2. Introduction

Nanoparticles (NPs) have been extensively studied over the past decades due to their unique chemical and physical properties.[1] Their intrinsic optical properties, in particular, have been widely exploited in biomedical applications.[2] For example, fluorescent nanoparticles such as quantum dots (QD) and carbon dots (CD) are used in bioimaging.[3,4] Additionally, plasmonic nanoparticles, such as gold nanoparticles (AuNPs) and silver nanoparticles (AgNPs), are applied in photothermal therapy[5], drug delivery[6] and sensing,[7] owing to their strong light absorption, with extinction coefficients exceeding 10^8 M^{-1} cm^{-1}, arising from their Localized Surface Plasmon Resonance (LSPR).[8] Other nanoparticles, including dye-doped latex beads, cellulose nanobeads, and magnetic iron oxide nanoparticles (IONPs), are also used in various biomedical applications and can exhibit interesting, though more limited, optical properties.[9]

For biomedical applications, nanoparticles must possess several key features. First, they must exhibit high stability in complex biological matrices, such as plasma or saliva. This stability is typically achieved by coating the NPs with an organic layer that electrostatically or sterically stabilizes the suspension.[10,11] Depending on the intended application, nanoparticles may be functionalized either by physisorption of polymers[12] or poly-charged molecules,[13] or by chemisorption, using, for example, thiol derivatives for noble metals[14] or phosphonic derivatives for metal oxides.[15] In this context, we introduced a covalent functionalization strategy based on the grafting of calix[4]arene tetra-diazonium salts.[16,17] These macrocyclic molecules can form multiple covalent bonds with metal surfaces, leading to a dense and thin organic layer that can be used to functionalize nanoparticles of various compositions and shapes.[18,19] This calixarene-based approach has been shown to surpass the traditional thiol chemistry in terms of stability and controlled composition of the coating.[20,21] Secondly, with the growing demand for precision nanomedicine, it is often necessary to target specific organs or cells, which requires the attachment of recognition units such as targeting antibodies, peptides or aptamers to the NPs.[22,23] For drug delivery applications, various (bio)molecules, such as nucleic acids, peptides, proteins or anticancer drugs can also be conjugated.[24,25] All these complex nanosystems are challenging to characterize, especially in regard to the confirmation of the presence of (bio)molecules on their surfaces and their quantification. Currently, bioconjugation characterization typically requires expensive and specialized equipment such as Nuclear Magnetic Resonance spectroscopy (NMR)[26,27], Inductively Coupled Plasma – Mass Spectrometry (ICP-MS)[28], thermogravimetric analysis[29] or are based on elemental analysis, which usually cannot accurately quantify the proportion of different (bio)molecules within complex coating layers.[30] Absorption and emission spectroscopic methods have also been described, however, these are only valid in specific cases or require ligand labelling.[31] Overall, these techniques provide limited information on bioconjugation efficiency, as most are only qualitative. They also frequently require a significant quantity of NPs or a fastidious sample treatment, making them unsuitable for rapid Quality Control (QC) analysis or bioconjugation process optimization.

Lateral Flow Assays (LFAs) offer numerous advantages, including low cost, rapid response, and ease of use.[32] They are among the most widely used point-of-care devices for detecting analytes such as viral proteins, antibodies and nucleic acids.[18,33–35] Recently, an LFA-type test was also used to discriminate the hybridization capabilities of various DNA aptamers conjugated to AuNPs.[36] In this context, we envisaged that LFAs could serve both to quickly confirm the presence of biomolecules on nanoparticles after a bioconjugation step and to quantify the amount of immobilized biomolecules. For this purpose, we developed a series of assays that provide detailed insights into the bioconjugation process and enable its optimization. Special emphasis was placed on designing a general characterization tool that can be used without specialized laboratory equipment, making this straightforward approach suitable for routine and rapid QC analysis of nanoparticle/biomolecule nanoconjugates.

3. Materials and Methods

3.1. Chemicals

All chemicals were at least of reagent grade. HP170 NC membranes were obtained from Cytiva while Absorbent Pads SureWick (1.7 × 30 cm^2) were purchased from Sigma-Aldrich. Anti-OVA polyclonal Antibody (pAb) (C6534), Ovalbumin and Protein G'(P4689) were ordered from Sigma Aldrich. OVA-Alexa647 were obtained from Invitrogen. cDNA-Biotin, HS-DNA, HS-RNA, and RNA were purchased from IDT (Leuven) and sequences are displayed in Table S1. Calix[4]arene $X_4(N_2^+)$ salt was purchased from X4C. AuNPs-citrate with a mean core diameter of 15 nm were synthesized and functionalized with calix[4]arene $X_4(N_2^+)$ salt leading to AuNPs-X_4 following a previously reported procedure.[37] AuNPs-S-DNA and AuNPs-S-RNA were produced based on a reported salts ageing procedure.[38]

3.2. Measurements

UV−vis absorption spectra were recorded with a UV−vis spectrophotometer in quartz cuvettes. As-synthesized NPs were diluted 10 times with deionized water, unless otherwise noted. Attenuated Total Reflection Fourier-Transform Infrared (ATR-FTIR) spectra were recorded at 20 °C on a Shimadzu QATR-S FTIR spectrophotometer. The nanoparticles were centrifugated, and 2 μL of the pellet were deposited on the diamond. Water was removed with a flow of nitrogen gas. Data were processed and analyzed using the instrument software by correcting the baseline and setting apodization at 10 cm^{-1}. An LFA dispenser from Claremont Bio was used to dispense the test line and ensure reproducibility.

3.3. Bioconjugation

Covalent Coupling. 500 µL of an AuNPs-X_4 suspension (OD=2.5) were added in a 1.5 mL glass vial. Then, 50 µL of MES buffer (100 mM, pH 5.8), 30 µL EDC.HCl (6 mM) and 30 µL Sulfo-NHS (10 mM) were successively added and the mixture was stirred for 1 hour. Then, the appropriate amount of OVA (100 µg/mL) or Rabbit IgG (100 µg/mL) was added and the mixture was stirred for 3 hours at room temperature (see Table VI-S2 for the volume of the OVA solution added as a function of the desired protein/NP ratio). The mixture was transferred to a 1.5 mL Protein Lobind Eppendorf and filled to 1.5 mL by adding phosphate buffer (10 mM, pH 7). After centrifugation at 18000 g for 20 minutes at room temperature, the supernatant was discarded, and the pellet was redispersed in 500 µL phosphate buffer (10 mM, pH 7). The resulting nanoparticles were stored at 4°C for further characterization.

Adsorption. 500 µL AuNPs-X_4 and 50 µL of phosphate buffer (100 mM, pH 6) were mixed in a 1.5 mL glass vial. Then, the appropriate amount of an OVA solution (100 µg/mL) was added, and the mixture was stirred for 3 hours at room temperature (see Table VI-S2 for the volume of the OVA solution added as a function of the desired protein/NP ratio). The mixture was transferred to a 1.5 mL Protein Lobind Eppendorf and filled to 1.5 mL by addition of phosphate buffer (10 mM, pH 7). After centrifugation at 18000 g for 20 minutes at room temperature, the supernatant was discarded, and the pellet was redispersed in 500 µL phosphate buffer (10 mM, pH 7). The resulting nanoparticles were stored at 4°C for further characterization.

3.4. Synthesis of AuNPs-S-DNA and AuNPs-S-RNA

AuNPs-citrate were functionalized with DNA or RNA single strands bearing a thiol group using the salt-aging method. Initially, the disulfide bridge of the thiolated DNA (SH-DNA) (or RNA (SH-RNA)) strands was cleaved with DTT 0.1 M in phosphate buffer saline (PBS). Then, SH-DNA (or RNA) strands were purified using a desalting column. After estimation of the quantity of purified nucleic acids by UV-visible absorption spectroscopy, DNA (or RNA) strands were added to AuNPs-citrate (OD = 8) through successive small additions to reach a final amount of 1000 SH-DNA (or RNA) strands/NP in the suspension. Finally, the NaCl concentration was increased by steps of 100 mM every 20 minutes until a final concentration of 500 mM. The mixture was then stirred overnight at room temperature. The particles were then washed by centrifugation four times with water at 15000 g for 20 minutes and the supernatant was removed.

3.5. Synthesis of AuNPs-S-RNAHyb

For the hybridization, the AuNPs conjugated with single RNA strand were mixed with 500 equivalents of the complementary RNA strand per particle in phosphate buffer (PB) 10 mM and 500 mM NaCl. The suspension was then heated at 65 °C for 10 minutes and allowed to return slowly to room temperature. After several hours, the mixture was centrifugated. The particles were finally resuspended in PBS and stored at 4°C.

3.6. Strip Assembly

Anti-OVA pAb (0.9 mg/mL) were immobilized on the nitrocellulose membrane as test line (T). The NC membrane was dried for 1 hour at 37°C. Then, the absorbent pad was added on the NC membrane (with an overlap of 2 mm). Dipstick were cut into 5-mm strips and stored in a desiccator. More detailed experimental information is given in SI.

Finding a universal control line for all systems compatible with such dipstick assays would be impossible; therefore, no control line was included. However, the proper functioning of the assay can be verified by visually monitoring particle elution and verifying complete sample absorption.

3.7. Assay Procedure

In a disposable cuvette, 40 µL of running buffer (1% BSA, 0.1% Tween 20 in 1X PBS) and 10 µL of AuNPs (OD=2) were mixed. The half strip was partially immersed into the solution and read-out was performed after 30 minutes. Isotype control experiment was performed similarly but a Rabbit IgG (dispensed at 1 mg/mL) strip were used instead of Anti-OVA strip.

3.8. Competitive Assay of Free OVA

5 µL of OVA (10 mg/mL) were mixed with 40 µL of running buffer. The anti-OVA strips were immersed in the solution during 5 minutes to allow the binding of free competitive OVA. Afterwards, 10 µL AuNPs-OVA (OD=2) were added in the solution. Read-out was performed after 25 minutes.

3.9.Quantification using Fluorescence of Ovalbumin

In a 1.5 mL glass vial, 500 µL of an AuNPs-citrate suspension (OD=2.5) (or 500 µL MilliQ water for calibration curve) and 20 µL of phosphate buffer (100 mM, pH 6) were added. Then, the appropriate volume of an OVA solution (100 µg/mL) was added, and the mixture was stirred for 3 hours at room temperature (see Table S2 for the volume of OVA added as function of number of eq/NP). Then, the suspension is transferred in a 1.5mL Eppendorf and centrifuged at 15000 g for 15 minutes at room temperature. 500 µL of supernatant were transferred in quartz cell and analyzed by emission spectroscopy exciting at 280 nm. Fluorescence intensity corresponds to the value at 330 nm.

3.10. Covalent Coupling Verification

In a 1.5 mL Eppendorf, 100 µL AuNPs (OD=2) were mixed with 100 µL SDS 1%wt for 15 minutes in a thermomixer at room temperature. Afterwards, the Eppendorfs were filled to 750 µL with deionized water and centrifuged at 18000g for 20 minutes. The dispersion/centrifugation cycle was repeated, and the pellet was ultimately redispersed in 200 µL of phosphate buffer (10 mM pH 7). Samples were stored at 4°C before use.

4. Results and Discussion

4.1. Synthesis and Characterization by IR and UV-vis Spectroscopy of AuNPs-OVA

To demonstrate the applicability of LFAs as a versatile tool for bioconjugation characterization, a nanoconjugate based on ovalbumin (OVA) immobilized on AuNPs was selected. OVA is commonly employed as a model antigen in early-stage vaccine development, while gold nanoparticles are extensively studied as drug delivery systems (DDS). Thus, designing a characterization tool that can i) validate the presence of OVA on the surface of AuNPs, and ii) quantify the amount of adsorbed OVA, would be a valuable proof of concept in the field of bioconjugation with nanosystems.[39,40]

15-nm AuNPs stabilized by citrate ligands were synthesized following a reported procedure.[41] These AuNPs-citrate were then functionalized with OVA by adsorption. To achieve this, a solution of OVA (50 OVA/NP ratio) was added to a suspension of AuNPs-citrate at pH 6, and the mixture was stirred for 3 hours. The resulting nanoparticles (AuNPs-OVA) were then centrifuged twice to remove any residual unbound proteins. Characterization of the resulting nanoparticles was performed using infrared (IR) spectroscopy and UV-vis absorption spectroscopy (Figure 1).

ATR-FTIR analysis of AuNPs-OVA confirmed the presence of OVA on the nanoparticles, as indicated by the intense signals corresponding to the amide I and II bands of the protein at 1650 and 1530 cm^{-1}, respectively (Figure 1, left). However, the signal intensities could not be reliably correlated with the amount of adsorbed proteins, as significant variations in the intensities of the amide bands were observed when samples were analyzed multiple times under identical conditions (Figure S1). This lack of reproducibility likely arises from the requirement to dry the particles on the detector, which can result in non-uniform deposition. Furthermore, any other adsorbed molecules, such as surface-blocking agents, may interfere with the IR analysis if their bands overlap with those of the adsorbed protein. In other words, while ATR-FTIR spectroscopy is convenient for qualitatively confirming the presence of adsorbed proteins, it is unreliable for quantitative analysis.

For UV-vis characterization, commercial ovalbumin labelled with the Alexa647 dye (OVA-Alexa647) was used for nanoparticle functionalization, resulting in AuNPs-OVA-Alexa647. The emission properties of dyes can be strongly influenced by their attachment to plasmonic nanoparticles,[42] making quantification by emission spectroscopy exceedingly difficult. Therefore, the characterization of AuNPs-OVA-Alexa647 was based on the absorption properties of the dye, which should be less affected upon adsorption on the NP surface (Figure 1, right). The protein dye-labelling approach can suffer from other limitations:

(i) the absorption spectrum of the dye must not overlap with that of the nanoparticles to allow quantification, which restricts the choice of compatible dyes;

(ii) commercially available dye-protein conjugates are not always precisely characterized. For instance, in our case, the OVA-Alexa647 datasheet specifies between 1 and 2 Alexa dyes per protein and an exact value cannot be determined, preventing accurate quantification;

(iii) when proteins are modified with dyes, the dye is typically conjugated to the lysine residues (as with the commercial OVA-Alexa647 used here), which precludes further coupling of the protein to nanoparticles via traditional amide bond formation and could influence the properties of the protein.

The UV-Vis absorption spectrum of AuNPs-OVA-Alexa647 exhibited a minor band at 647 nm corresponding to the dye present at the NP surface (Figure 1, right). However, the very low intensity of this signal prevented reliable quantification, given the weak absorption coefficient of the dye compared to that of AuNPs and the small number of proteins that can be adsorbed on the metallic surface. An amount of 15-30 OVA/NP was roughly estimated, based on the intensity of the Alexa absorption and the datasheet characterization.

All these results show that IR or UV-vis absorption spectroscopy are neither reliable nor convenient for quantifying the number of biomolecules bound to the nanoparticles and can only be used for qualitative analysis.

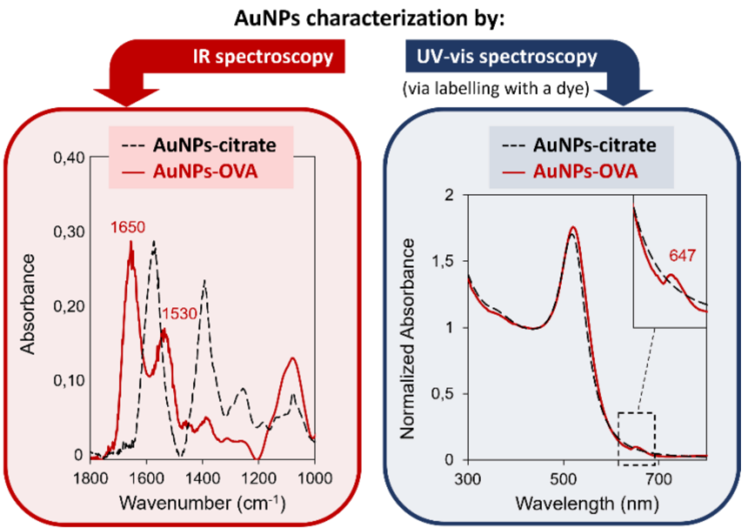

Figure 1. Characterization of AuNPs-OVA (solid red line) and AuNPs-citrate (black dashed line) by infrared spectroscopy (left) or UV-vis absorption spectroscopy (right).

4.2. Use of LFAs as a Characterization and Quantification Tool

LFAs, particularly half-strip assays, a simplified version of the Lateral Flow Assay composed solely of the nitrocellulose (NC) membrane and the adsorbent pad, can be very easily prepared and require only inexpensive consumables (Figure 2A). For the recognition process at the Test line (T line), a solution of commercially available antibodies or aptamers targeting the biomolecule conjugated to the nanoparticles can be dispensed on the backed NC membrane, either manually (using a syringe or a volumetric pipette) or with an automated LFA dispenser. Following this step, the NC card is dried at 37°C for 1 hour, after which the absorbent pad is added. The card is then sliced into strips that can simply be stored in a desiccator for long-term use (see the SI for more details on strip assembly and alternative protocols). Noteworthy, a single NC card yields approximately 50 strips, which remain stable for months. In this study, different techniques to dispense the T line on the half-strips intended for AuNPs-OVA characterization (i.e. Anti-OVA strips) were compared: the anti-OVA IgG solution was deposited on the NC membrane using an automated LFA dispenser or by manual deposition using either a syringe or a micropipette.

A typical characterization procedure involved partially immersing the lower extremity of an Anti-OVA half-strip into a solution of AuNPs-OVA diluted in a running buffer (1% BSA, 0.1%wt Tween 20 in 1X PBS) with a final optical density (OD) of 0.4 for 30 minutes (Figure 2B). Note that, unlike traditional sandwich LFAs, the functionalized AuNPs bind directly to the antibody deposited on the T line, eliminating the need for the formation of a sandwich complex to generate the visible colored signal. This straightforward operational principle avoids the need for laborious fine-tuning of test conditions, particularly the buffer composition, which is crucial in sandwich assays to ensure optimal conditions for the formation of the ternary complex. Regardless of the dispensing method (syringe, micropipette, or automated LFA dispenser), a clear red signal was consistently observed at the T line (Figure 2C). Note that for all the following studies, the T line was dispensed using an automated LFA dispenser, as this technique is required to allow reproducible protein deposition on the T line and quantification of the signal intensity. No false positive results were obtained with AuNPs-citrate, demonstrating specificity for OVA-functionalized particles. As shown in Table 1, the assay tolerates a wide variety of chemicals interferents, even at high concentrations (see Figure S2 for pictures of the corresponding positive and negative control assays). Note that the interferent concentrations were selected based on standard working concentrations reported in the literature for sandwich-like assays. This absence of interference from blocking agents, buffer components, or residual reagents in the NP solution is due to the specificity of the recognition process, a key advantage of this characterization tool over FTIR or emission spectroscopy.

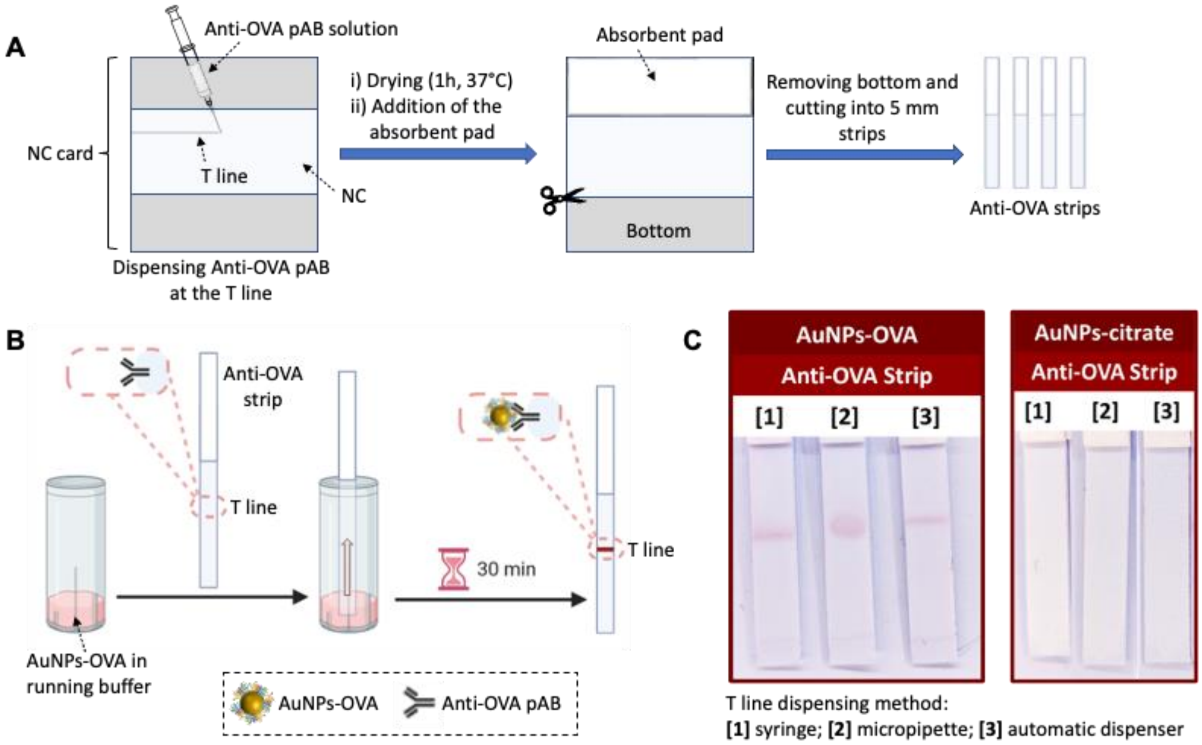

Figure 2. (A) Manual preparation of Anti-OVA strips; (B) Principle of the LFA characterization of AuNPs-OVA; (C) Pictures of Anti-OVA strips after testing AuNPs-OVA and AuNPs-citrate prepared using different T line dispensing methods: [1] syringe, [2] micropipette, and [3] automatic dispenser.

Table 1. Assay tolerance to potential interfering substances. "Tolerable Concentration" refers to the final concentration in the assay.

Interfering substances	Tolerable Concentration
SDS	0.1 wt%
Triton X-100	0.1 wt%
DTT	10 mM
EDTA	2 mM
$CaCl_2$	2 mM
Sucrose	0.5 wt%
NaN_3	10 mM
TRIS.HCl (pH 7)	10 mM

To rule out non-specific interactions between AuNPs-OVA and the rabbit IgG on the strip line, control experiments were conducted using a rabbit IgG that does not interact with ovalbumin. As shown in Figure S3A, no line was observed on these strips with AuNPs-OVA. Further validation was performed by saturating the anti-OVA IgG on the test line with a 1 mg/mL ovalbumin solution before applying AuNPs-OVA. As displayed in Figure S3B, this treatment resulted in the disappearance of the signal, further confirming the specificity of the interaction. This approach provides a simple and effective control for the development of new characterization assays.

We then investigated the quantification of the number of proteins bound per NP. To this end, various batches of AuNPs-OVA were prepared by mixing AuNPs-citrate with different OVA/NP ratios (from 0 to 100) for 3 hours. Since the T line contained a large excess of Anti-OVA pAb relative to the number of NPs used in each test (>10^4 Anti-Ova pAb per NP), all the resulting NPs batches were directly tested with the Anti-OVA strip assay without cleaning the particles from unbound OVA proteins. This simple procedure avoids potential experimental errors and long cleaning cycles. As displayed in Figure 3A, a faint red line was observed from 5 eq. OVA/NP, and then the color intensity of the band increased with the OVA/NP ratio, reaching a plateau between 20 and 25 eq. (see Figure S4A-B for all the experiments and duplicates). Signal intensity for each strip was quantified using a previously reported procedure based on the ImageJ software (Figure 3B).[43] Quantitative analysis confirmed the naked eye observations, with a linear relationship between the number of OVA equivalents added to the suspension during the functionalization step and the signal intensity from 5 to 25 equivalents and a plateau observed higher OVA/NP ratios. This value is in good agreement with the theoretical maximum number of OVA per NP, assuming a dense monolayer of OVA on the NP surface (see SI for calculation). Notably, the observed plateau cannot be attributed to a competition between AuNPs-OVA and unbound OVA at the level of the T line, given the large excess of immobilized Anti-Ova pAb (*vide supra*).

To confirm these results, the AuNPs-OVA samples with varying OVA equivalents per NP were centrifuged, and the quantity of OVA remaining in the supernatant was estimated by fluorescence spectroscopy. Fluorescence emission intensity was measured at the maximal emission wavelength of OVA (330 nm) following excitation at 280 nm (see Figure S5 for all the fluorescence spectra). A calibration curve using pure OVA solutions was also established using the same protocol (incubation and centrifugation) but in the absence of AuNPs (Figure 3C, black dots), allowing us to correlate the emission intensity of the OVA signal in the supernatants with the corresponding protein quantity. Fluorescence of OVA could be detected in the supernatant only from the 15 eq. OVA/NP sample (Figure 3C- red dots). Considering the difference of fluorescence between the control (pure OVA) and the supernatant of OVA-NPs, we estimated that approximately 15-20 OVA are adsorbed per NP at the plateau, which aligns well with the value obtained via the LFA. This experiment confirmed the suitability of LFAs for quantifying protein loading on the NP surface. It should be noted that this fluorescence method is appropriate only in specific cases of bioconjugation, such as adsorption, where no other organic molecules, such as coupling reagents, that could absorb light at the same wavelength as the functionalization ligand are present. In addition, this indirect method measures proteins remaining in the supernatant rather than those directly bound to the NPs.

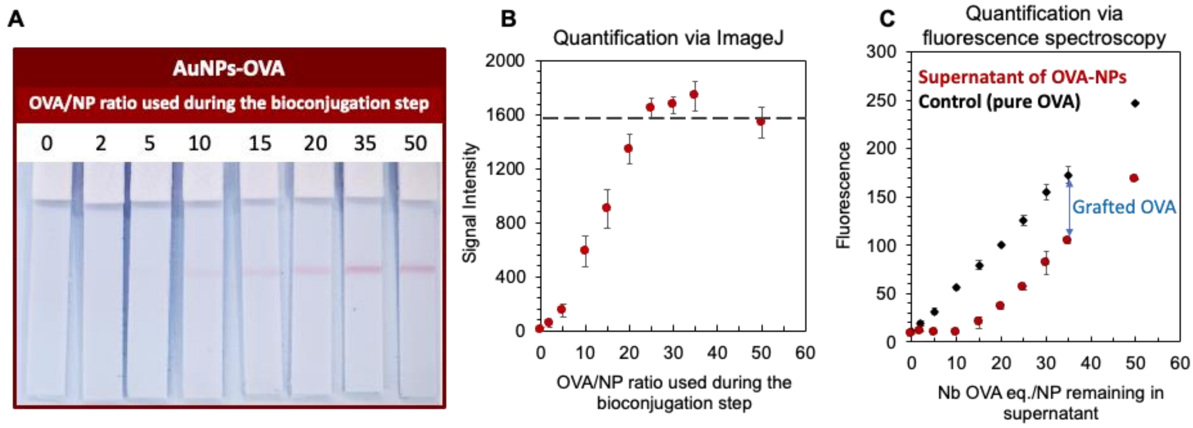

Figure 3: (A) Picture of Anti-OVA strips after testing different batches of AuNPs-OVA prepared with varying OVA/NP ratios (from 0 to 50, corresponding to a molar concentration ranging from 0 to 290 nM) during the bioconjugation step. The final concentration of AuNPs-citrate during the bioconjugation step is approximately 6 nM. (B) Quantification of T line signal intensity using ImageJ, error bars correspond to the standard deviation calculated on minimum three repetitions of each measurement; (C) Fluorescence intensity at 330 nm (excitation at 280 nm) of OVA in the supernatant after conjugation with (red) and without (black) AuNPs in the reaction mixture. Error bars correspond to the standard deviation calculated on three repetitions of each measurement.

4.3. Application to Complex Nanosystems

Having validated the suitability of LFAs to confirm protein adsorption on gold nanoparticles and quantify the number of adsorbed proteins, we decided to illustrate that this simple assay can be used to optimize new bioconjugation protocols. As a proof of concept, we chose to characterize the covalent coupling of OVA to calix[4]arene-coated nanoparticles (Figure 4A). Calix[4]arene-coated nanoparticles, namely AuNPs-X_4, were first prepared following a reported procedure involving the reduction of the tetradiazonium calix[4]arene salt $X_4(N_2^+)_4$ in the presence of 15 nm AuNPs-citrate (see Figure S6).[37] OVA was then covalently conjugated to AuNPs-X_4 under standard coupling conditions (EDC/Sulfo-NHS), yielding AuNPs-X_4-OVA^{Cov} (Figure 4A). For comparison, nanoparticles obtained through the adsorption of OVA on AuNPs-X_4, referred to AuNPs-X_4-OVA^{Ads}, were also prepared. In both cases, different batches of NPs were prepared by varying the OVA/NP ratio during the bioconjugation step (ratios of 10, 50, and 150). The LFA characterization of the various batches of NPs was then performed with Anti-OVA strips (Figures 4B and 4C) according to the procedure described previously (Figure 2). A signal intensity proportional to the OVA/NP ratio was observed. AuNPs-X_4-OVA^{Cov} exhibited a more intense red line compared to AuNPs-X_4-OVA^{Ads}, particularly at higher protein-to-NP ratios. This result is likely related to the potential formation of protein multilayers via the EDC/sulfo-NHS coupling chemistry, as peptide bonds can form between proteins, thereby increasing the probability of binding events and enhancing AuNPs immobilization at the test line.

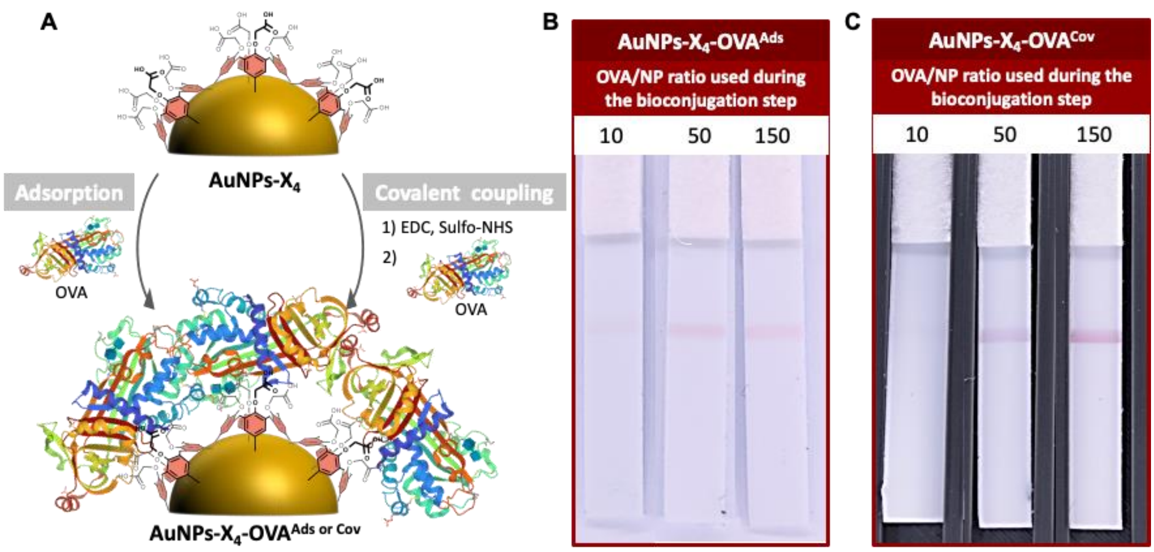

Figure 4: (A) Preparation of AuNPs-X_4-OVA by adsorption (AuNPs-X_4-OVA^{Ads}) or covalent bonding (AuNPs-X4-OVA^{Cov}); Pictures of Anti-OVA strips after testing AuNPs-X_4-OVA^{Ads} (B) and AuNPs-X_4-OVA^{Cov} (C) prepared with various OVA/NP ratios during the conjugation step.

The use of LFAs was also evaluated for optimizing the covalent conjugation conditions of OVA to the NPs. For instance, performing the amide bond formation at pH 5.8 in MES buffer was significantly more efficient than at pH 8.5 in borate buffer, as demonstrated by the more intense signal intensity at the T line under these conditions (Figure 5A). This simple optimization approach could be extended to various parameters, such as NP and reagent concentrations or the number of steps for the conjugation (Figures S7). Overall, rapid and straightforward testing of bioconjugation conditions could be realized by running a simple LFA.

Finally, we investigated the possibility of discriminating AuNPs-X_4-OVA^{Ads} from AuNPs-X_4-OVA^{Cov} using our LFA. To achieve this, the NPs were treated with sodium dodecyl sulfate

(SDS) (final concentration 0.5%) for 15 minutes to detach adsorbed proteins. After centrifugation to remove excess SDS, the resulting NPs were analyzed using anti-OVA strips (Figure 5B). A drastic decrease in signal intensity was observed after the SDS cleaning step for the nanoparticles on which the OVA was adsorbed, indicating that most of the protein was removed from the surface. On the contrary, the SDS cleaning step had no effect on the signal intensity for AuNPs-X_4-OVA^{Cov}, confirming the covalent attachment of the protein. These results show that a simple SDS treatment followed by LFA analysis can reliably determine whether a biomolecule is covalently linked to a NP or merely adsorbed on its surface.

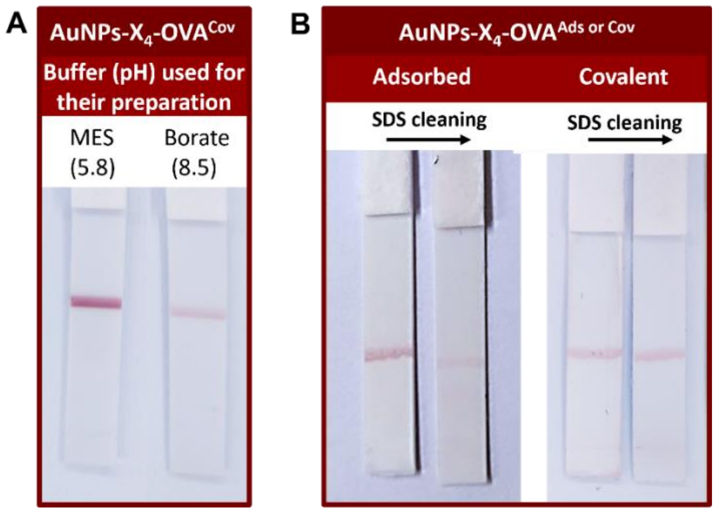

Figure 5: (A) Pictures of Anti-OVA strips after testing AuNPs-X_4-OVA^{Cov} prepared in two different buffers; (B) Pictures of Anti-OVA strips before and after SDS cleaning of AuNPs-X_4-OVA$^{Ads\ or\ Cov}$.

4.4. Extension of the Assay to antibodies and nucleic acids

Finally, we extended our approach to the detection of antibodies and nucleic acids immobilized on nanoparticles, as these biomolecules, along with antigen proteins, constitute the majority of biomolecules used to functionalize nanoparticles for biomedical applications. For detecting antibodies immobilized on NPs, covalent nanoconjugates between Rabbit IgG and AuNPs-X_4, namely AuNPs-X_4-IgG^{Cov}, were prepared using the standard EDC/Sulfo-NHS procedure (see the Experimental Section). A test line containing Protein G was used, given its high binding affinity for the heavy chain of antibodies.[44] LFA analysis of AuNPs-X_4-Rabbit IgG^{Cov} produced an intense red signal at the T line, while no signal was observed in the control experiment with AuNPs-X_4 alone (Figure 6A), demonstrating that LFAs can be used to confirm the immobilization of antibodies on nanoparticles.

To detect oligonucleotides on NPs, the complementary strand cannot be directly immobilized at the test line, due to its low molecular weight. We therefore used a strategy we recently employed for immobilizing peptide aptamers on a NC strip, which involves coupling streptavidin, as a carrier protein, to the biotinylated molecule to immobilize.[45] Briefly, the biotinylated complementary DNA (cDNA-biotin) strand was incubated with streptavidin for 30 minutes and then directly dispensed on the NC membrane (see Supporting Information for the detailed information on the cDNA strip assembly). As a proof-of-concept, AuNPs functionalized with either thiolated DNA or RNA strands were prepared. We selected one DNA (DNA^{C}) and one RNA (RNA^{C}) sequence complementary to the one deposited on the strip (cDNA strip), as well as a DNA control sequence (DNA^{NC}) with no complementarity to the cDNA strip. The resulting AuNPs-S-DNA^{C}, AuNPs-S-RNA^{C}, and AuNPs-S-DNA^{NC} were characterized using the cDNA strips (Figures 6B and 6C). A positive red line was observed for both AuNPs-S-DNA^{C} and AuNPs-S-RNA^{C}, highlighting the high specificity of the system for both DNA- and RNA-functionalized NPs. Notably, in the case of AuNPs-S-RNA^{C}, the positive test indicates that a DNA-RNA hybrid duplex was formed. Finally, when AuNPs-S-RNA^{C} were hybridized with their free complementary strand, forming a double stranded RNA (RNA^{Hyb}) on the particle surface, a significant decrease in signal intensity was observed (Figure 6C). This result confirms successful hybridization, a particularly valuable finding for researchers preparing particles with double-stranded nucleic acids for cell delivery applications, as verifying hybridization at the surface of the particles is known to be particularly challenging. To demonstrate the broad applicability of the assay, we also performed bioconjugation of OVA onto various nanoparticles, gold nanorods, 40-nm gold nanoparticles and silver nanoplates, with different optical properties and confirmed OVA adsorption using the anti-OVA strip (see Figure S8).

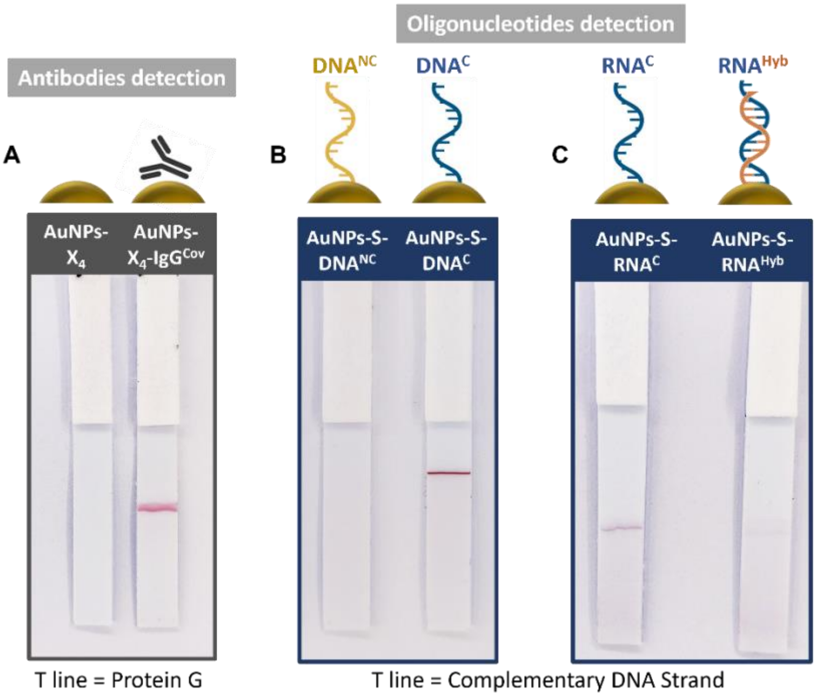

Figure 6: (A) Picture of Protein G strips after testing AuNPs-X_4 and AuNPs-X_4-Rabbit IgG^{Cov}; (B) and (C) Pictures of cDNA strips after testing various AuNPs conjugated to thiolated oligonucleotides.

5. Conclusion

In this work, we demonstrated the successful development of accessible half-strip assays to characterize nanoparticles conjugated with various biomolecules. It is worth mentioning that such assays restricted to particles that exhibit efficient light absorption or scattering properties in the visible range. These assays were designed without the need for costly equipment and required only minimal nanoparticle quantities. Importantly, they provide a range of critical information about both the bioconjugation process and the properties of the final nanoconjugates:

i) they enable unambiguous confirmation of the presence of biomolecules, such as proteins, antibodies, and oligonucleotides, on the nanoparticle surface;

ii) they distinguish between biomolecules covalently linked to the nanoparticle surface and those simply adsorbed onto it;

iii) they facilitate the optimization of conditions for effective covalent coupling between a biomolecule and a nanoparticle;

iv) they allow for precise quantification of the number of biomolecules bound per nanoparticle;

v) they can readily differentiate nanoparticles coated with RNA duplexes from those coated with single-stranded RNA.

These findings underscore the assay's potential as a straightforward, versatile tool for characterizing complex nanosystems at various stages of preparation, significantly advancing the toolkit available for nanoparticle functionalization and quality control in biomedical and biochemical applications.

Supporting information

LFA assembly procedure, FTIR spectra, fluorescence spectra, pictures of half-strips, structures of calix[4]arene $X_4(N_2^+)_4$ and thiol-terminated nucleic acids.

Conflicts ofinterest

The authors declare no competing financialinterest.

ACKNOWLEDGMENTS

This research was supported by the Fonds pour la formation à la Recherche dans l'Industrie et dans l'Agriculture (FRIA-FRS) and the Fonds David et Alice Van Buuren (PhD grant to B.G.). The authors thank the "Fondation Jaumotte-Demoulin" for the acquisition of the equipment necessary for the preparation of the LFA strips.

References

(1) Ahlawat, J.; Hooda, R.; Sharma, M.; Kalra, V.; Rana, J. S.; Batra, B. Nanoparticles in Biomedical Applications. In *Green Nanoparticles*; Patra, J. K., Fraceto, L. F., Das, G., Campos, E. V. R., Eds.; Nanotechnology in the Life Sciences; Springer International Publishing: Cham, 2020; pp 227–250. https://doi.org/10.1007/978-3-030-39246-8_11.

(2) Rezić, I. Nanoparticles for Biomedical Application and Their Synthesis. *Polymers* **2022**, *14* (22), 4961. https://doi.org/10.3390/polym14224961.

(3) Han, X.; Xu, K.; Taratula, O.; Farsad, K. Applications of Nanoparticles in Biomedical Imaging. *Nanoscale* **2019**, *11* (3), 799–819. https://doi.org/10.1039/C8NR07769J.

(4) Li, W.; Kaminski Schierle, G. S.; Lei, B.; Liu, Y.; Kaminski, C. F. Fluorescent Nanoparticles for Super-Resolution Imaging. *Chem. Rev.* **2022**, *122* (15), 12495–12543. https://doi.org/10.1021/acs.chemrev.2c00050.

(5) Vines, J. B.; Yoon, J.-H.; Ryu, N.-E.; Lim, D.-J.; Park, H. Gold Nanoparticles for Photothermal Cancer Therapy. *Front. Chem.* **2019**, *7*, 167. https://doi.org/10.3389/fchem.2019.00167.

(6) Kong, F.-Y.; Zhang, J.-W.; Li, R.-F.; Wang, Z.-X.; Wang, W.-J.; Wang, W. Unique Roles of Gold Nanoparticles in Drug Delivery, Targeting and Imaging Applications. *Molecules* **2017**, *22* (9), 1445. https://doi.org/10.3390/molecules22091445.

(7) Gosselin, B.; Retout, M.; Dutour, R.; Troian-Gautier, L.; Bevernaegie, R.; Herens, S.; Lefèvre, P.; Denis, O.; Bruylants, G.; Jabin, I. Ultrastable Silver Nanoparticles for Rapid Serology Detection of Anti-SARS-CoV-2 Immunoglobulins G. *Anal. Chem.* **2022**, *94* (20), 7383–7390. https://doi.org/10.1021/acs.analchem.2c00870.

(8) Kelly, K. L.; Coronado, E.; Zhao, L. L.; Schatz, G. C. The Optical Properties of Metal Nanoparticles: The Influence of Size, Shape, and Dielectric Environment. *J. Phys. Chem. B* **2003**, *107* (3), 668–677. https://doi.org/10.1021/jp026731y.

(9) Sakurai, A.; Takayama, K.; Nomura, N.; Yamamoto, N.; Sakoda, Y.; Kobayashi, Y.; Kida, H.; Shibasaki, F. Multi-Colored Immunochromatography Using Nanobeads for Rapid and Sensitive Typing of Seasonal Influenza Viruses. *Journal of Virological Methods* **2014**, *209*, 62–68. https://doi.org/10.1016/j.jviromet.2014.08.025.

(10) Thanh, N. T. K.; Green, L. A. W. Functionalisation of Nanoparticles for Biomedical Applications. *Nano Today* **2010**, *5* (3), 213–230. https://doi.org/10.1016/j.nantod.2010.05.003.

(11) Jin, Z.; Yeung, J.; Zhou, J.; Retout, M.; Yim, W.; Fajtová, P.; Gosselin, B.; Jabin, I.; Bruylants, G.; Mattoussi, H.; O'Donoghue, A. J.; Jokerst, J. V. Empirical Optimization of Peptide Sequence and Nanoparticle Colloidal Stability: The Impact of Surface Ligands and Implications for Colorimetric Sensing. *ACS Appl. Mater. Interfaces* **2023**, *15* (16), 20483–20494. https://doi.org/10.1021/acsami.3c00862.

(12) Zhang, F.; Lees, E.; Amin, F.; RiveraGil, P.; Yang, F.; Mulvaney, P.; Parak, W. J. Polymer-Coated Nanoparticles: A Universal Tool for Biolabelling Experiments. *Small* **2011**, *7* (22), 3113–3127. https://doi.org/10.1002/smll.201100608.

(13) Bastús, N. G.; Comenge, J.; Puntes, V. Kinetically Controlled Seeded Growth Synthesis of Citrate-Stabilized Gold Nanoparticles of up to 200 Nm: Size Focusing versus Ostwald Ripening. *Langmuir* **2011**, *27* (17), 11098–11105. https://doi.org/10.1021/la201938u.

(14) Salamone, T. A.; Rutigliano, L.; Pennacchi, B.; Cerra, S.; Matassa, R.; Nottola, S.; Sciubba, F.; Battocchio, C.; Marsotto, M.; Del Giudice, A.; Chumakov, A.; Davydok, A.; Grigorian, S.; Canettieri, G.; Agostinelli, E.; Fratoddi, I. Thiol Functionalised Gold

Nanoparticles Loaded with Methotrexate for Cancer Treatment: From Synthesis to in Vitro Studies on Neuroblastoma Cell Lines. *Journal of Colloid and Interface Science* **2023**, *649*, 264–278. https://doi.org/10.1016/j.jcis.2023.06.078.

(15) Wan, J.; Yuan, R.; Zhang, C.; Wu, N.; Yan, F.; Yu, S.; Chen, K. Stable and Biocompatible Colloidal Dispersions of Superparamagnetic Iron Oxide Nanoparticles with Minimum Aggregation for Biomedical Applications. *J. Phys. Chem. C* **2016**, *120* (41), 23799–23806. https://doi.org/10.1021/acs.jpcc.6b06614.

(16) Valkenier, H.; Malytskyi, V.; Blond, P.; Retout, M.; Mattiuzzi, A.; Goole, J.; Raussens, V.; Jabin, I.; Bruylants, G. Controlled Functionalization of Gold Nanoparticles with Mixtures of Calix[4]Arenes Revealed by Infrared Spectroscopy. *Langmuir* **2017**, *33* (33), 8253–8259. https://doi.org/10.1021/acs.langmuir.7b02140.

(17) Mattiuzzi, A.; Jabin, I.; Mangeney, C.; Roux, C.; Reinaud, O.; Santos, L.; Bergamini, J.-F.; Hapiot, P.; Lagrost, C. Electrografting of Calix[4]Arenediazonium Salts to Form Versatile Robust Platforms for Spatially Controlled Surface Functionalization. *Nat Commun* **2012**, *3* (1), 1130. https://doi.org/10.1038/ncomms2121.

(18) Retout, M.; Gosselin, B.; Adrović, A.; Blond, P.; Jabin, I.; Bruylants, G. Ultra-Stable Silver Nanoplates: Efficient and Versatile Colorimetric Reporters for Dipstick Assays. *Nanoscale* **2023**, *15* (28), 11981–11989. https://doi.org/10.1039/D3NR02378H.

(19) Retout, M.; Jabin, I.; Bruylants, G. Synthesis of Ultrastable and Bioconjugable Ag, Au, and Bimetallic Ag_Au Nanoparticles Coated with Calix[4]Arenes. *ACS Omega* **2021**, *6* (30), 19675–19684. https://doi.org/10.1021/acsomega.1c02327.

(20) Troian-Gautier, L.; Valkenier, H.; Mattiuzzi, A.; Jabin, I.; Den Brande, N. V.; Mele, B. V.; Hubert, J.; Reniers, F.; Bruylants, G.; Lagrost, C.; Leroux, Y. Extremely Robust and Post-Functionalizable Gold Nanoparticles Coated with Calix[4]Arenes via Metal–Carbon Bonds. *Chem. Commun.* **2016**, *52* (69), 10493–10496. https://doi.org/10.1039/C6CC04534K.

(21) Retout, M.; Blond, P.; Jabin, I.; Bruylants, G. Ultrastable PEGylated Calixarene-Coated Gold Nanoparticles with a Tunable Bioconjugation Density for Biosensing Applications. *Bioconjugate Chem.* **2021**, *32* (2), 290–300. https://doi.org/10.1021/acs.bioconjchem.0c00669.

(22) Mitchell, M. J.; Billingsley, M. M.; Haley, R. M.; Wechsler, M. E.; Peppas, N. A.; Langer, R. Engineering Precision Nanoparticles for Drug Delivery. *Nat Rev Drug Discov* **2021**, *20* (2), 101–124. https://doi.org/10.1038/s41573-020-0090-8.

(23) Alghamdi, M. A.; Fallica, A. N.; Virzì, N.; Kesharwani, P.; Pittalà, V.; Greish, K. The Promise of Nanotechnology in Personalized Medicine. *JPM* **2022**, *12* (5), 673. https://doi.org/10.3390/jpm12050673.

(24) Afzal, O.; Altamimi, A. S. A.; Nadeem, M. S.; Alzarea, S. I.; Almalki, W. H.; Tariq, A.; Mubeen, B.; Murtaza, B. N.; Iftikhar, S.; Riaz, N.; Kazmi, I. Nanoparticles in Drug Delivery: From History to Therapeutic Applications. *Nanomaterials* **2022**, *12* (24), 4494. https://doi.org/10.3390/nano12244494.

(25) Dykman, L. A. Gold Nanoparticles for Preparation of Antibodies and Vaccines against Infectious Diseases. *Expert Review of Vaccines* **2020**, *19* (5), 465–477. https://doi.org/10.1080/14760584.2020.1758070.

(26) Toti, U. S.; Guru, B. R.; Grill, A. E.; Panyam, J. Interfacial Activity Assisted Surface Functionalization: A Novel Approach To Incorporate Maleimide Functional Groups and cRGD Peptide on Polymeric Nanoparticles for Targeted Drug Delivery. *Mol. Pharmaceutics* **2010**, *7* (4), 1108–1117. https://doi.org/10.1021/mp900284c.

(27) Retout, M.; Brunetti, E.; Valkenier, H.; Bruylants, G. Limits of Thiol Chemistry Revealed by Quantitative Analysis of Mixed Layers of Thiolated-PEG Ligands Grafted onto Gold Nanoparticles. *Journal of Colloid and Interface Science* **2019**, *557*, 807–815. https://doi.org/10.1016/j.jcis.2019.09.047.

(28) Fernández-Iglesias, N.; Bettmer, J. Complementary Mass Spectrometric Techniques for the Quantification of the Protein Corona: A Case Study on Gold Nanoparticles and Human Serum Proteins. *Nanoscale* **2015**, *7* (34), 14324–14331. https://doi.org/10.1039/C5NR02625C.

(29) Bouchoucha, M.; Béliveau, É.; Kleitz, F.; Calon, F.; Fortin, M.-A. Antibody-Conjugated Mesoporous Silica Nanoparticles for Brain Microvessel Endothelial Cell Targeting. *J. Mater. Chem. B* **2017**, *5* (37), 7721–7735. https://doi.org/10.1039/C7TB01385J.

(30) Oliverio, R.; Liberelle, B.; Murschel, F.; Garcia-Ac, A.; Banquy, X.; De Crescenzo, G. Versatile and High-Throughput Strategy for the Quantification of Proteins Bound to Nanoparticles. *ACS Appl. Nano Mater.* **2020**, *3* (10), 10497–10507. https://doi.org/10.1021/acsanm.0c02414.

(31) Slesiona, N.; Payne, L.; Pope, I.; Borri, P.; Langbein, W.; Watson, P. Correlative Extinction and Single Fluorophore Bleaching Microscopy for Ligand Quantification on Gold Nanoparticles. **2022**. https://doi.org/10.48550/ARXIV.2210.00942.

(32) Di Nardo, F.; Chiarello, M.; Cavalera, S.; Baggiani, C.; Anfossi, L. Ten Years of Lateral Flow Immunoassay Technique Applications: Trends, Challenges and Future Perspectives. *Sensors* **2021**, *21* (15), 5185. https://doi.org/10.3390/s21155185.

(33) Jauset-Rubio, M.; Svobodová, M.; Mairal, T.; McNeil, C.; Keegan, N.; Saeed, A.; Abbas, M. N.; El-Shahawi, M. S.; Bashammakh, A. S.; Alyoubi, A. O.; O´Sullivan, C. K. Ultrasensitive, Rapid and Inexpensive Detection of DNA Using Paper Based Lateral Flow Assay. *Sci Rep* **2016**, *6* (1), 37732. https://doi.org/10.1038/srep37732.

(34) Zeng, L.; Li, Y.; Liu, J.; Guo, L.; Wang, Z.; Xu, X.; Song, S.; Hao, C.; Liu, L.; Xin, M.; Xu, C. Rapid, Ultrasensitive and Highly Specific Biosensor for the Diagnosis of SARS-CoV-2 in Clinical Blood Samples. *Mater. Chem. Front.* **2020**, *4* (7), 2000–2005. https://doi.org/10.1039/D0QM00294A.

(35) Li, X.; Sun, F.; Chang, R.; Xie, Z.; Peng, C.; Zhang, Y.; Wang, Z.; Liu, G. A Versatile Strategy of Designing Gold Nanoparticle–cDNA Nanoprobes in Developing Aptamer-Based Lateral Flow Assay for Small-Molecule Detection. *Langmuir* **2023**, *39* (25), 8690–8697. https://doi.org/10.1021/acs.langmuir.3c00645.

(36) Huang, M.; Xiong, E.; Wang, Y.; Hu, M.; Yue, H.; Tian, T.; Zhu, D.; Liu, H.; Zhou, X. Fast Microwave Heating-Based One-Step Synthesis of DNA and RNA Modified Gold Nanoparticles. *Nat Commun* **2022**, *13* (1), 968. https://doi.org/10.1038/s41467-022-28627-8.

(37) Retout, M.; Gosselin, B.; Jokerst, J. V.; Jabin, I.; Bruylants, G. A Fluoride-Induced Aggregation Test to Quickly Assess the Efficiency of Ligand Exchange Procedures from Citrate Capped AuNPs. *Colloids and Surfaces A: Physicochemical and Engineering Aspects* **2023**, *660*, 130801. https://doi.org/10.1016/j.colsurfa.2022.130801.

(38) Hurst, S. J.; Lytton-Jean, A. K. R.; Mirkin, C. A. Maximizing DNA Loading on a Range of Gold Nanoparticle Sizes. *Anal. Chem.* **2006**, *78* (24), 8313–8318. https://doi.org/10.1021/ac0613582.

(39) Jia, Y.; Akache, B.; Agbayani, G.; Chandan, V.; Dudani, R.; Harrison, B. A.; Deschatelets, L.; Hemraz, U. D.; Lam, E.; Régnier, S.; Stark, F. C.; Krishnan, L.; McCluskie, M. J. The Synergistic Effects of Sulfated Lactosyl Archaeol Archaeosomes When Combined with Different Adjuvants in a Murine Model. *Pharmaceutics* **2021**, *13* (2), 205. https://doi.org/10.3390/pharmaceutics13020205.

(40) Chang, T. Z.; Stadmiller, S. S.; Staskevicius, E.; Champion, J. A. Effects of Ovalbumin Protein Nanoparticle Vaccine Size and Coating on Dendritic Cell Processing. *Biomater. Sci.* **2017**, *5* (2), 223–233. https://doi.org/10.1039/C6BM00500D.

(41) Doyen, M.; Bartik, K.; Bruylants, G. UV–Vis and NMR Study of the Formation of Gold Nanoparticles by Citrate Reduction: Observation of Gold–Citrate Aggregates. *Journal of Colloid and Interface Science* **2013**, *399*, 1–5. https://doi.org/10.1016/j.jcis.2013.02.040.

(42) Dulkeith, E.; Ringler, M.; Klar, T. A.; Feldmann, J.; Muñoz Javier, A.; Parak, W. J. Gold Nanoparticles Quench Fluorescence by Phase Induced Radiative Rate Suppression. *Nano Lett.* **2005**, *5* (4), 585–589. https://doi.org/10.1021/nl0480969.

(43) Parolo, C.; Sena-Torralba, A.; Bergua, J. F.; Calucho, E.; Fuentes-Chust, C.; Hu, L.; Rivas, L.; Álvarez-Diduk, R.; Nguyen, E. P.; Cinti, S.; Quesada-González, D.; Merkoçi, A. Tutorial: Design and Fabrication of Nanoparticle-Based Lateral-Flow Immunoassays. *Nat Protoc* **2020**, *15* (12), 3788–3816. https://doi.org/10.1038/s41596-020-0357-x.

(44) Boi, C. Membrane Adsorbers as Purification Tools for Monoclonal Antibody Purification. *Journal of Chromatography B* **2007**, *848* (1), 19–27. https://doi.org/10.1016/j.jchromb.2006.08.044.

(45) Gosselin, B.; Retout, M.; Jabin, I.; Bruylants, G. Development of a Peptide-Based Lateral Flow Assay for the Detection of the Cancer Biomarker Mdm2. *Sens. Diagn.* **2024**, 10.1039.D3SD00253E. https://doi.org/10.1039/D3SD00253E.